SOLAR P-MODE CHARACTERISTICS ASSOCIATED WITH SUPERACTIVE-REGIONS OBSERVED DURING OCT–NOV 2003

Ashok Ambastha[1], Sarbani Basu[2], H. M. Antia[3], and R. S. Bogart[4]

[1]*Udaipur Solar Observatory, Physical Research Laboratory, P. O. Box 198, Udaipur 313001, India*
[2]*Astronomy Department, Yale University, P. O. Box 208101, New Haven CT 06520-8101, U. S. A.*
[3]*Tata Institute of Fundamental Research, Homi Bhabha Road, Mumbai 400005, India*
[4]*CSSA-HEPL, Stanford University, Stanford, CA 94305-4085, U. S. A.*

ABSTRACT

Extensive flare activity was observed in super-active region NOAA 10486 during its disk passage of October 22–November 04, 2003. We have applied the ring diagram analysis technique to 3-D power spectra obtained for this active region in order to study any possible effect of these large flares on properties of the p-modes. The two other large, but relatively less flare productive active regions, viz., NOAA 10484, and NOAA 10488 observed during this period have also been included for comparison with NOAA 10486. In the flaring active region, we found mode power enhancement, and steep gradient in the meridional velocity, as compared to the quiet regions.

Key words: Sun: Activity; Sun: Oscillations; Sun: Interior.

1. INTRODUCTION

Solar flares are amongst the most energetic phenomena observed on the solar surface. There are observations suggesting that some large flares may excite waves on the solar surface (Kosovichev & Zharkova 1998, 1999). Recently, we analysed MDI data obtained for several active regions of the current solar cycle that produced flares of varying magnitude. In most cases, during the period of high flare activity, power in p-modes appears to be larger when compared to that in non-flaring regions of similar magnetic field strength (Ambastha et al. 2003). During October–November 2003 in the decay phase of this cycle, three large active regions NOAA 10484, 10486 and 10488 appeared on the Sun. Amongst these, the superactive region NOAA 10486 produced flares of unprecedented magnitude. In this work we wish to study the effect of these flares on p-mode oscillation characteristics using the ring diagram technique (Hill 1988; Patrón et al. 1997; Basu et al. 1999) applied to 3D spectra from data obtained by the Michelson Doppler Imager (MDI).

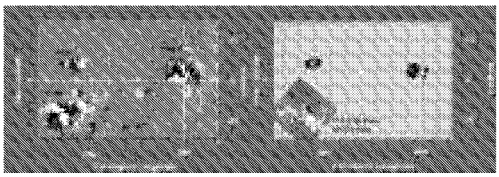

Figure 1. The magnetic polarity or flux distribution (left panels), and intensity images (right panels) of solar active regions NOAA 10484, 10486 and 10488. H_α filtergram showing the X17.2/4B flare is overlaid on the intensity image of NOAA 10486, using sunspots as reference.

2. FLARES AND THE ACTIVE REGIONS

The superactive region NOAA 10486 produced in quick succession flares of extremely large magnitude, i.e., X5.4/1B, X17.2/4B, X10/2B, X8.3/2B, and also the record setting X28/3B flare. Unfortunately, the largest flare observed in this region was not suitable for our study as by this time the active region had reached the West limb. On the other hand, NOAA 10484 and 10488 were comparatively dormant although they too grew to large sunspot areas. Table 1 lists the physical characteristics of the active regions, *viz.*, area, and the magnetic class. Also listed are the details of the major flares observed in these active regions, *viz.*, importance of the flare in X-ray/H_α, its location, the start and end times of the flares. We have calculated flare indices (FI) for the selected active region using the quantity $Q = i \times \tau$ to quantify the daily flare activity summed over the duration of tracked data sets using the method described by Kleczek (1952), and Atac & Özgüc (1998). In this relation, i is the intensity scale of the importance, and τ is the duration of the flare in minutes.

The magnetic flux distribution and corresponding intensity images of the selected active regions as obtained from MDI synoptic charts are shown in Fig. 1. Fig. 2 shows the spatial and temporal development of the X17.2/4B flare as seen using H_α filtergrams. The observations were

Proceedings of the SOHO 14 / GONG 2004 Workshop, New Haven, Connecticut, USA, 12-16 July 2004
(ESA SP-559, October 2004)

Table 1. Characteristics of solar Active Regions (AR) and Flares.

Date Oct 03	Area ($10^{-6} A_\odot$)	Mag. Class	Flare Class SXR/H_α	Location Flare/AR	Start (UT)	End (UT)
Active region NOAA 10484						
20	1367	bgd		N05E48		
21	1715			N05E34		
22	1982	bgd		N04E22		
23	1815	bgd	M3.2/1N	N04E13	07:05	07:18
24	1612	bgd	M1.0/1N	N05W09	21:38	21:48
25	1824	bgd		N03W19		
26	1576	bgd	X1.2/1N	N02W38	17:21	19:21
			M7.6/2N	N01W38	21:26	22:26
27	1410	bgd	M2.7/2F	N00W45	07:46	09:32
Active region NOAA 10486						
25	2479	bgd	M1.2/2N	S15E43	04:15	07:09
26	2340	bgd	X1.2/3B	S17E38	05:57	08:50
27	2172	bgd		S16E24		
28	2126	bgd	X17.2/4B	S16E08	09:51	14:20
29	2582	bgd	M1.1/1F	S18W08	00:29	02:39
			X10.0/2B	S15W13	20:37	22:53
30	2395	bgd		S18W15		
31	2210	bgd		S17W28		
Active region NOAA 10488						
26	0091	b		N07E23		
27	0293	bg		N09E16		
28	0787	bgd		N08E04		
29	1648	bgd		N08W07		
30	1669	bgd	M1.6/1N	N08W22	01:53	02:54
31	1724	bgd		N08W34		

Table 2. Regions studied using ring diagram analysis

No.	Carr. Rot	Lat. Lon.	CM Lon.	Start time	End time	MAI	FI
R01	2008	7.5N	030	10.20/16:49	10.21/20:32	126	147
R02		352.5	015	10.21/20:08	10.22/23:51	140	166
R03	2009		360	10.22/23:26	10.24/03:09	148	45
R04			345	10.24/02:45	10.25/06:28	154	83
R05			330	10.25/06:04	10.26/09:47	145	10
R06			315	10.26/09:22	10.27/13:05	127	494
R11	2009	15S	315	10.26/09:22	10.27/13:05	209	41
R12		285	300	10.27/12:41	10.28/16:24	223	1111
R13			285	10.28/16:00	10.29/19:43	232	267
R14			270	10.29/19:18	10.30/23:01	228	350
R15			255	10.30/22:37	11.01/02:20	215	37
R21	2009	7.5N	330	10.25/06:04	10.26/09:47	1	0
R22		292.5	315	10.26/09:22	10.27/13:05	19	9
R23			300	10.27/12:41	10.28/16:24	74	168
R24			285	10.28/16:00	10.29/19:43	125	68
R25			270	10.29/19:18	10.30/23:01	142	66
R26			255	10.30/22:37	11.01/02:20	147	89

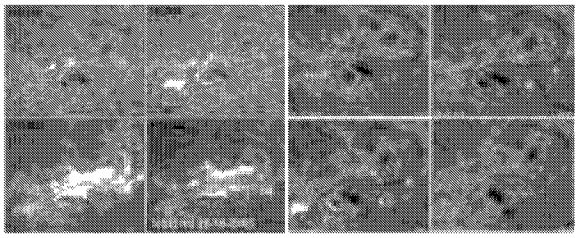

Figure 2. The spatial and temporal development of the 4B/X17.2 flare observed in NOAA 10486. After the flare of October 28, 2003, some parts of the filament 'c' have reformed, and 'd' has disappeared.

taken at the Udaipur Solar Observatory (USO) at a cadence of 3 seconds during the flare. The flare was impulsive in nature. Post-flare loops formed in the decay phase of this two ribbon flare. Preflare brightenings at "a" and "b" before the major flare and the eruption of large portion of the filament "c" are also seen. This flare was a long duration event (LDE) lasting over 4.5 hours. Fig. 2 also shows the daily evolution of NOAA 10486 during the period October 26–31, 2003. Several structural changes are seen in the filaments which delineate magnetic polarity reversal lines in the AR. Changes appear to be associated with reconnection process after the X17/4B flare of October 28, 2003.

In order to study the effect of flares on solar oscillation modes, we use the ring diagram analysis technique on data sets from MDI as listed in Table 2. Each of the data sets covers a region of about $16° \times 16°$ on the Sun and a time interval of 1664 minutes. We have chosen the data from available sets when the active region was close to the central meridian. The table gives the heliographic coordinates of the central point as well as the central meridian longitude at midpoint in time. It also gives a measure of average surface magnetic field in the region in the form of Magnetic Activity Index (MAI) (see Basu et al. 2004 for definition) as well as the Flare Index defined above. For convenience each region is identified by the serial number listed in the first column. To fit the 3d spectra we use a model with asymmetric peak profiles as used by Basu & Antia (1999). The mode characteristics we are interested in are the frequency, peak power, half-width and the horizontal velocities.

3. RESULTS

Fig. 3 summarises the results for each of the 3 ARs that we have studied. The upper panels show the evolution of amplitude and width of modes. The amplitude and width are averaged over all modes in frequency range of 2.5–3 mHz for f-modes ($n = 0$) and over 3–3.5 mHz for p-modes. All differences shown in the figures are with respect to the first region. For the active region NOAA 10486 the largest FI occurred in region R12, when the region was close to the central meridian. The FI was dominated by the contribution from the long duration event, i.e., X17.2/4B flare. The magnetic field was increasing

slowly around that time. Even then the mode-amplitudes are larger than those during region R11 before the flare. After this major flare there were other large flares for the next two days (including an X10/2B) and the amplitude increased even more. Figure 4 shows the difference in mode characteristics in the region covered by NOAA 10486 at different times. The frequencies and widths are not significantly affected during this period.

Active region NOAA 10484 had its largest flare during the last region covered in this study. By this time the magnetic field had started decreasing. The amplitude shows a steady increase with time, which may be unrelated to flares. Active region NOAA 10488 started developing only around the central meridian passage as the magnetic field increased sharply, and the FI was high in R23 due to the contribution from several small flares. In this case although the amplitude appears to be decreasing with time, but if we account for the sharp increase in magnetic field the effective amplitude after correction for MAI would increase. There is also a steep variation in the width of modes, probably due to magnetic field variation.

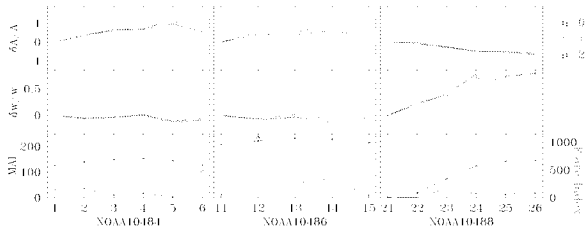

Figure 3. The evolution of MAI and flare index for each of the regions is compared with evolution of mode characteristics like, amplitude and width of modes. The horizontal axis is the serial number of the region, which is generally at an interval of about 1 day.

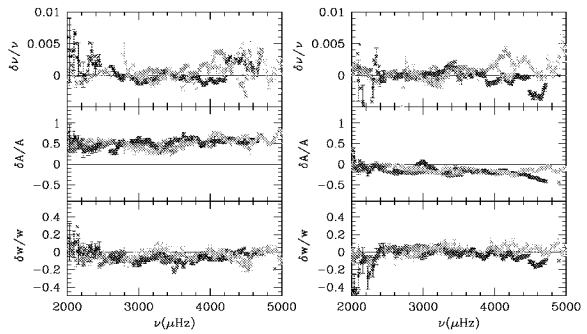

Figure 4. The relative difference in mode frequencies, and widths as well as ratio of peak power for NOAA 10486. The left and right panels respectively, show the difference between regions $R12 - R11$ (preflare), and $R12 - R14$ (postflare). The red, green, blue and cyan points respectively, show the modes with $n = 0, 1, 2, 3$. For clarity, error bars are shown for a few representative modes only.

Since the amplitude of oscillations is also affected by magnetic field (e.g., Rajaguru et al. 2001) we need to filter out this effect before considering the effect of flares.

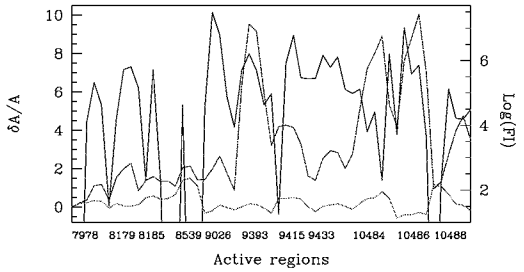

Figure 5. Variations in the average amplitude (for $n = 0, 1, 2, 3$) of p-modes for the 11 active regions shown as a function of serial numbers of the regions, though for convenience the axis is marked with the identification of the active regions. The black curve shows $\log(FI)$ on the scale marked on the right axis. The red curve shows $\delta(\log A)$ while the blue curve shows the same after correcting for MAI.

This can be done by adding the quantity MAI/80 to the difference in logarithm of amplitude (Rajaguru et al. 2001). Figure 5 summarises the results for different active regions studied by us, including those studied earlier (Ambastha et al. 2003). This figure shows the average variation in amplitude for each active region. The amplitude differences are taken with respect to a region covered by NOAA 7978 when there was no flare and it had very low magnetic field. The differences are averaged over all f-modes ($n = 0$) in frequency range 2.5–3 mHz and p-modes ($n = 1, 2, 3$) in the frequency range 3–3.5 mHz. The amplitude differences corrected for the magnetic field are also shown by blue line in the figure. It can be seen that after accounting for variation in MAI, most active regions studied by us show enhancement of power in p-modes due to flares as the peaks in FI and in amplitude are found to be correlated in time. However, the amplitude does not seem to have any obvious correlation with magnitude of FI.

Apart from amplitudes, the velocity along the horizontal directions is also calculated by ring diagram fits and it would be interesting to check if there is any variation in the velocity due to flares or if the flaring regions show different velocity profile as compared to other regions. The fitted velocities for each mode can be inverted to calculate the zonal and meridional components of velocity as a function of depth. We have used both Regularized Least Squares (RLS) and Optimally Localised Averages (OLA) techniques for inversions and the results are shown in Fig. 6. It appears that in flaring regions the meridional velocity has a steep gradient below a depth of 4 Mm. For NOAA 9026, the meridional velocity shows a steep gradient in regions R40–R41, when flares occurred, and this gradient has disappeared in R44 after the flares. In NOAA 10484 the gradient is much less. In NOAA 10488 there is no u_y gradient in regions R21, R22 as the active region had not yet emerged. After that the gradient developed as the active region is formed and the flare took place. Apart from the meridional component the subsurface shear layer normally present in the zonal component

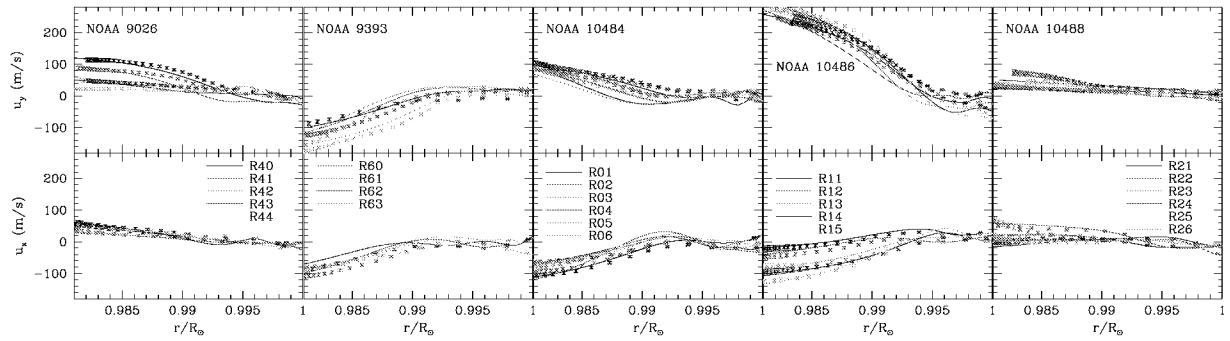

Figure 6. The zonal (u_x) and meridional (u_y) components of velocity for active regions NOAA 9026, 9393, 10484, 10486 and 10488 at different stages. The lines show the results obtained using RLS inversions, while points mark those obtained using OLA. For NOAA 9026 and 9393 the regions marked are listed in Table IV of Ambastha et al. (2003).

seems to have disappeared in flaring regions. Amongst the results shown here only NOAA 9026 has some shear layer.

Following Basu et al. (2004) we also attempt to study possible difference in structure in these active regions and quiet regions at same latitude. In order to get better spectra, we track the regions for 8192 minutes around the central meridian passage. We also select a quiet region at the same latitude and during the same Carrington rotation for comparison. The resulting frequency differences are inverted using the RLS and OLA techniques to calculate the difference in sound speed between an active and a quiet region. The results are shown in Fig. 7 for the three active regions considered here. These differences are similar to those in other non-flaring active regions.

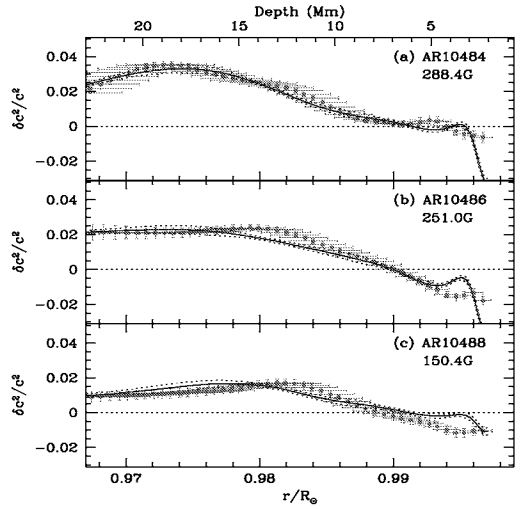

Figure 7. The difference in sound speed squared between an active and quiet region as inferred using RLS (blue lines) and OLA (red points) inversion techniques for active regions NOAA 10484, 10486 and 10488.

4. CONCLUSIONS

During the large X17/4B flare in NOAA 10486, the power in acoustic modes appears to increase beyond the normal value expected from the influence of magnetic field. This is as also seen in other flaring regions studied earlier. The meridional velocity in flaring region appears to have a steep gradient below a depth of 4 Mm. It is not clear if this is real or an artifact of degradation of spectra during flares. Nevertheless, occurrence of this gradient is somewhat correlated to flares. The sound speed difference between an active and quiet region shows that sound speed is lower in the active region just below the surface, but at depths exceeding 7 Mm the trend reverses.

ACKNOWLEDGMENTS

This work utilises data from the Solar Oscillations Investigation / Michelson Doppler Imager (SOI/MDI) on the Solar and Heliospheric Observatory (SOHO). SOHO is a project of international cooperation between ESA and NASA. MDI is supported by NASA grants NAG5-8878 and NAG5-10483 to Stanford University. This work was supported by NASA grant NAG5-10912 to SB.

REFERENCES

Ambastha A., Basu S., Antia H. M., 2003, Solar Phys. 218, 151

Atac T., Özgüc A., 1998, Solar Phys. 180, 397

Basu S., Antia H. M., 1999, ApJ 525, 517

Basu S., Antia H. M., Tripathy S. C., 1999, ApJ 512, 458

Basu S., Antia H. M., Bogart R. S., 2004, ApJ 610, 1157

Hill F., 1988, ApJ 333, 996

Kleczek J., 1952, Publ. Inst. Centr. Astron. Prague, No. 22

Kosovichev A. G., Zharkova V. V., 1998, Nature 393, 317

Kosovichev A. G., Zharkova V. V., 1999, Solar Phys. 190, 459

Patrón J., González Hernández I., Chou D.-Y., et al. 1997, ApJ 485, 869

Rajaguru S. P., Basu S., Antia H. M., 2001, ApJ 563, 410